Developing the family of picolinate ligands for Mn^{2+} complexation[†]

Attila Forgács[a], Rosa Pujales-Paradela[b], Martín Regueiro-Figueroa[b], Laura Valencia[c], David Esteban-Gómez[b], Mauro Botta[a] and Carlos Platas-Iglesias[b]

[a] Dipartimento di Scienze e Innovazione Tecnologica, Università del Piemonte Orientale "A. Avogadro", Viale T. Michel 11, 15121 Alessandria, Italy

[b] Universidade da Coruña, Centro de Investigacións Científicas Avanzadas (CICA) and Departamento de Química Fundamental, Facultade de Ciencias, 15071, A Coruña, Galicia, Spain

[c] Departamento de Química Inorgánica, Facultad de Ciencias, Universidade de Vigo, As Lagoas, Marcosende, 36310 Pontevedra, Spain

How to cite:

Abstract

We have reported here a series of ligands containing pentadentate 6,6′-(azanediylbis(methylene))dipicolinic acid units that differ in the substituent present at the amine nitrogen atom (acetate: H$_3$DPAAA; phenyl: H$_2$DPAPhA; dodecyl: H$_2$DPAC12A; 4-hexylphenyl: H$_2$DPAC6PhA). The protonation constants of the hexadentate DPAAA^{3-} and pentadentate DPAPhA^{2-} ligands and the stability constants of their Mn^{2+} complexes were determined using pH-potentiometry (25 °C, 0.15 M NaCl). The mono-hydrated [Mn(DPAAA)]$^-$ complex (log K_{MnL} = 13.19(5)) was found to be considerably more stable than the bis-hydrated [Mn(DPAPhA)] analogue (log K_{MnL} = 9.55(1)). A detailed ^{1}H and ^{17}O NMR relaxometric study was carried out to determine the parameters that govern the proton relaxivities of these complexes. The [Mn(DPAC12A)] complex, which contains a dodecyl lipophilic chain, forms micelles in solution characterized by a critical micellar concentration (cmc) of 96(9) μM. The lipophilic [Mn(DPAC6PhA)] and [Mn(DPAC12A)] derivatives form rather strong adducts with Human Serum Albumin (HSA) with association constants of 7.1 ± 0.1 × 10^3 and 1.3 ± 0.4 × 10^5 M^{-1}, respectively. The X-ray structure of the complex {K(H$_2$O)$_4$}{[Mn(DPAAA)(H$_2$O)]}$_2$ shows that the Mn^{2+} ion in [Mn(DPAAA)]$^-$ is coordinated to the six donor atoms of the ligand, a coordinated water molecule completing the pentagonal bipyramidal coordination environment.

Introduction

In recent years, the stable complexation of Mn^{2+} in aqueous solution has been attracting increasing attention due to the potential application of high-spin complexes of this metal ion as contrast enhancing agents in magnetic resonance imaging (MRI).[1,2] Mn^{2+} salts were among the first compounds to be used as contrast

agents to distinguish normal myocardial tissue from infarcted zones in animals.[3] However, the advent of rather efficient Gd^{3+}-based contrast agents (CA) developed during the 1980s and 1990s concentrated most of the research efforts of the MRI community on this class of agents.[4] As a result, only one Mn^{2+} CA has been approved for clinical use (mangafodipir trisodium, $Na_3[Mn(H_3DPDP)]$, TESLASCAN®, Scheme 1).[5] This hepatocyte specific MRI contrast agent releases Mn^{2+}, which is sequestered by the liver, providing an enhanced contrast for diagnostic imaging.[6] However, some toxicity problems associated with the administration of Gd^{3+}-based MRI CAs[7] have renewed the interest in Mn^{2+} agents,[8–10] which are expected to have a better toxicity profile.[1]

The design of Mn^{2+}-based MRI contrast agents represents a challenge for coordination chemistry. Indeed, a Mn^{2+} complex should fulfil a number of requirements to become a potential CA candidate: (i) a high thermodynamic and kinetic stability to avoid the release of the toxic Mn^{2+} ions. The lack of a crystal field stabilization energy associated with the high-spin d^5 configuration results in rather low thermodynamic stabilities of Mn^{2+} complexes, which are also generally rather labile with respect to complex dissociation;[11] (ii) the presence of at least one water molecule coordinated to the metal ion that exchanges rapidly with the bulk water, thereby imparting an efficient pathway to accelerate the relaxation rates of water proton nuclei. It is worth noting that Mn^{2+} chelates with high thermodynamic stability such as $[Mn(DOTA)]^{2-}$ and $[Mn(DO3A)]^-$ do not contain coordinated water molecules;[12] (iii) a good redox stability to avoid the oxidation of Mn^{2+} to Mn^{3+}, which generally provides lower relaxivities. However, redox Mn^{2+}/Mn^{3+} potentials accessible to biologically relevant reducing agents can be potentially exploited to design redox-activated MRI probes.[13,14]
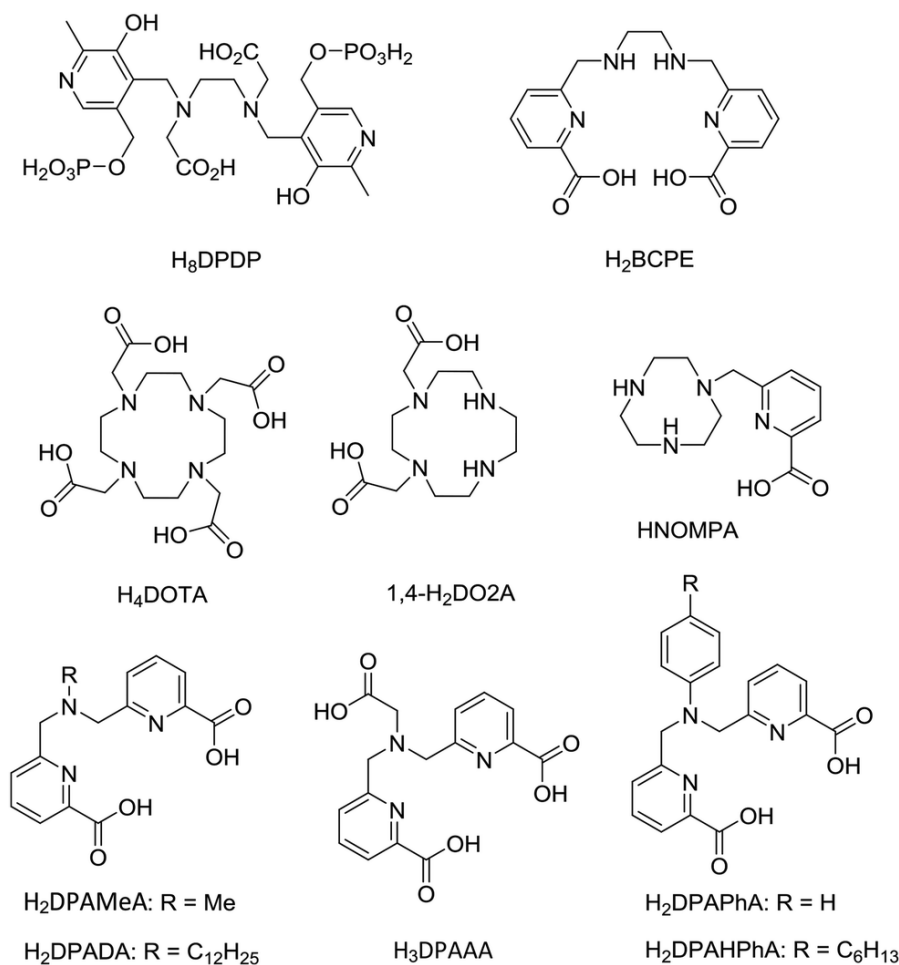

Scheme 1. Structures of the ligands discussed in this work.

In recent papers, we have reported the pentadentate ligand H$_2$DPAMeA[15] and derivatives bearing two or three H$_2$DPAMeA binding motifs for the formation of bi- and tri-nuclear Mn^{2+} entities.[16] These complexes contain two water molecules coordinated to the metal ions, which results in relatively high relaxivities. Furthermore, the observed ^{1}H relaxivities increased considerably in plasma due to binding to human serum albumin (HSA). However, the Mn^{2+} complex formed by the H$_2$BCPE ligand does not contain inner-sphere water molecules, which highlights the difficulty of predicting the hydration numbers for this family of complexes. Herein, we expand the family of ligands containing picolinate groups by reporting the pentadentate ligand H$_2$DPAPhA and the hexadentate derivative H$_3$DPAAA. The latter ligand was reported previously by Mazzanti and colleagues and investigated in the context of Gd^{3+} MRI CAs.[17] Furthermore, we also report two lipophilic derivatives of H$_2$DPAMeA and H$_2$DPAPhA, which contain a dodecyl side chain attached to the amine nitrogen atom of H$_2$DPAMeA or a hexyl chain at the aniline function of H$_2$DPAPhA, respectively. These lipophilic derivatives were designed to form micelles in solution and to bind HSA in a non-covalent fashion. Both effects are expected to increase the observed relaxivity by slowing down the rotation of the complex in solution. We report the synthesis and acid–base properties of the ligands, the stability constants of the Mn^{2+} complexes in solution, and a full physicochemical characterization of the chelates using ^{1}H and ^{17}O relaxometric techniques and theoretical (DFT) calculations.

Results and discussion

Synthesis of the ligands

The ligands reported in this work were prepared following the two-step procedure shown in Scheme 2. The first step consisted in the reaction of 6-chloromethylpyridine-2-carboxylic acid ethyl ester with an appropriate amine in the presence of K$_2$CO$_3$ as a base. It is worth mentioning that the reactions with anilines required rather harsh conditions involving heating for prolonged periods and the addition of catalytic KI. The ester intermediates were isolated in rather good yields (65–72%) after purification using column chromatography. Hydrolysis of the ethyl ester groups (and the amide group of the precursor of H$_3$DPAAA) provided the target ligands as the hydrochloride salts in good overall yields (52–61%).
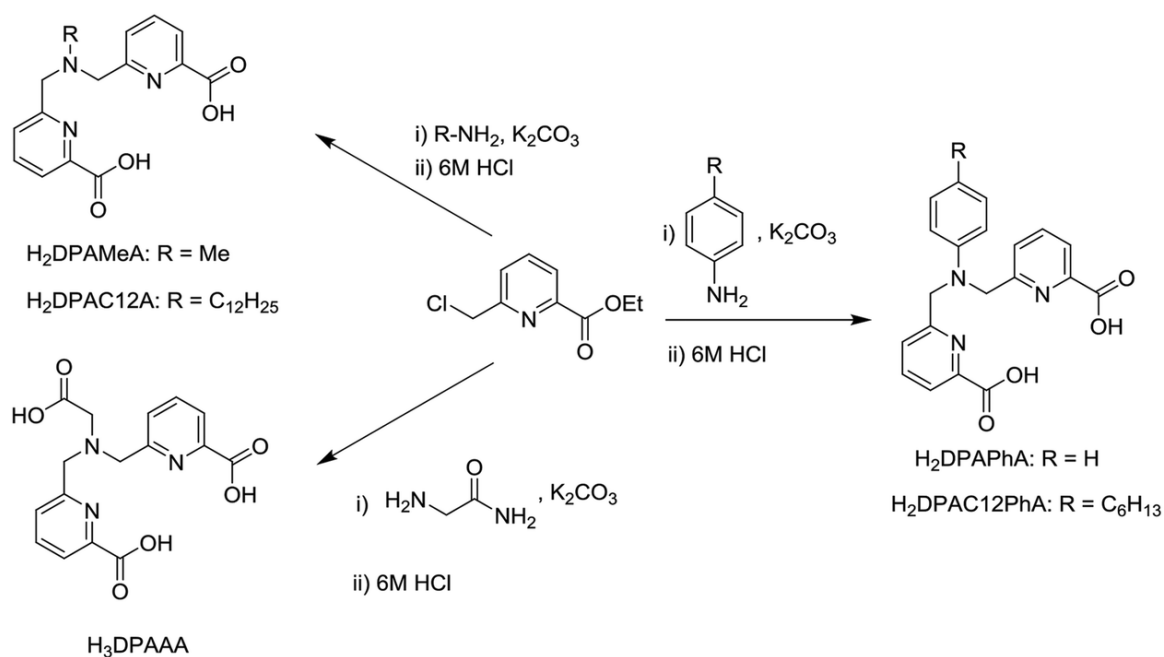
Scheme 2. Synthesis of the ligands.

Ligand protonation constants and stability constants of the Mn^{2+} complexes

The protonation constants of DPAPhA^{2-} and DPAAA^{3-} were determined by potentiometric titrations in 0.15 M NaCl. The ligand protonation constants are defined in eqn (1):

$$K_i^H = \frac{[H_iL]}{[H_{i-1}L][H^+]} \text{ with } i = 1,2,3,4. \tag{1}$$

The protonation constants together with their corresponding standard deviations are compiled in Table 1.

Table 1. Ligand protonation constants and stability and protonation constants of the corresponding Mn^{2+} complexes determined using potentiometric titrations (25 °C, 0.15 M NaCl)

	DPAAA^{3-}	DPAPhA^{2-}	DPAMeA$^{2-\ a}$	EDTA$^{4-\ b}$
log K_1^H	7.26(2)	5.48(4)	7.82	10.17
log K_2^H	3.90(3)	4.51(4)	3.71	6.11
log K_3^H	3.29(2)	4.28(4)	2.61	2.68
log K_4^H	1.77(2)	2.70(4)		
$\sum$log K_i^H	16.22	16.97	14.14	
log K_{MnL}	13.19(5)	9.55(1)	10.13	13.88
log K_{MnLH}	2.90(6)	4.84(1)	2.57	
log K_{MnLH_2}		2.51(1)		
log K_{MLOH}	11.97(6)		11.09	
pMn^c	8.98	7.27	7.28	7.95

^{a} Data from ref. 16. ^{b} Data from ref. 19. c Defined as $-\log[Mn]_{free}$ with pH = 7.4, $[Mn^{2+}] = [L] = 10^{-5}$ M.

Four protonation constants could be determined for DPAAA^{3-}, indicating the stepwise protonation of the amine nitrogen atom and all three carboxylate groups of the ligand. The first and second protonation constants of DPAAA^{3-} are very similar to those reported previously for DPAMeA^{2-}. These protonation processes are assigned to the protonation of the amine nitrogen atom (K_1^H) and one of the carboxylate groups of the picolinate arms (K_2^H). The first protonation constant of DPAPhA^{2-} (log K_1^H = 5.48(4)) is *ca.* two orders of magnitude lower than those determined for DPAAA^{3-} and DPAMeA^{2-}, in line with the lower basicity of anilines compared to aliphatic amines.[18] Four protonation constants could be determined for DPAPhA^{2-}, indicating the protonation of the aniline nitrogen atom, two carboxylate groups and likely a nitrogen atom of a pyridine moiety. As a result, the DPAAA^{3-} and DPAPhA^{2-} ligands present very similar overall basicities, as estimated by the $\sum$log K_i^H values (i = 1–4). The protonation constants determined for DPAAA^{3-} in 0.15 M NaCl are in good agreement with those reported by Mazzanti in 0.1 M KCl (log K_1^H = 7.33, log K_2^H = 3.8 and log K_3^H = 2.9).[17]

The stability and protonation constants of the Mn^{2+} complexes of DPAAA^{3-} and DPAPhA^{2-} were determined using direct potentiometric pH-titrations. The stability constants and protonation constants of the complexes are defined in eqn (2) and (3):

$$K_{\mathrm{ML}} = \frac{[\mathrm{ML}]}{[\mathrm{M}][\mathrm{L}]} \tag{2}$$

$$K_{\mathrm{H}_i\mathrm{L}} = \frac{[\mathrm{MH}_i\mathrm{L}]}{[\mathrm{MH}_{i-1}\mathrm{L}][\mathrm{H}^+]} \text{ with } i = 1, 2. \tag{3}$$

The titration curve of the Mn^{2+}:DPAAA^{3-} system evidenced the formation of a hydroxo complex characterized by the protonation constant K_{MLOH} defined as:

$$K_{\mathrm{MLOH}} = \frac{[\mathrm{ML}]}{[\mathrm{ML(OH)}][\mathrm{H}^+]} \tag{4}$$

The stability constant of the [Mn(DPAPhA)] complex is slightly lower than that reported previously for [Mn(DPAMeA)], which is likely related to the weaker coordination of the aniline nitrogen atom of DPAPhA^{2-} compared to the amine nitrogen atom of DPAMeA^{2-} (see computational details below). The presence of an additional carboxylate group in DPAAA^{3-} increases the stability of the Mn^{2+} complex by three orders of magnitude with respect to DPAMeA^{2-}. As a result, the stability constant of the [Mn(DPAAA)]$^-$ complex (log K_{ML} = 13.19(5)) approaches that of the EDTA analogue (log K_{ML} = 13.88).[19]

Fig. 1 presents the species distribution diagrams calculated using the equilibrium constants reported in Table 1. The [Mn(DPAAA)]$^-$ species is the most abundant one in a wide range of pH from *ca.* 2.8 to 11.4. The formation of the hydroxo [Mn(DPAAA)(OH)]$^{2-}$ species occurs above pH $\sim$ 10, while the protonation of the complex is observed below pH $\sim$ 5.0. Dissociation of the complex takes place at a rather low pH, with only 5.6% of the manganese in the form of [Mn(H$_2$O)$_6$]$^{2+}$ at pH 2.0.

The dissociation of [Mn(DPAPhA)] starts at higher pH than that of [Mn(DPAAA)]$^-$, as 27.8% of the complex is dissociated at pH 2.0. However, the degree of dissociation of the complex at pH 2.0 is even higher in the case of [Mn(DPAMeA)] (77.7%).[16] [Mn(DPAPhA)] forms protonated species at rather high pH (<7.0).

A comparison of the thermodynamic stabilities of complexes with different ligands is more appropriately given by the pMn values (pMn = $-\log[\mathrm{Mn}^{2+}]_{\mathrm{free}}$) defined using the conditions suggested by Drahos[20] (pH = 7.4, [Mn^{2+}] = [L] = 10^{-5} M). The pMn values calculated for [Mn(DPAMeA)] and [Mn(DPAPhA)] are virtually identical (7.3, Table 1) and somewhat lower than that of [Mn(EDTA)]$^{2-}$. The latter complex serves as a reference for potential MRI applications, as [Mn(EDTA)]$^{2-}$ derivatives have been successfully used in *in vivo* MRI studies.[21] Interestingly, the [Mn(DPAAA)]$^-$ complex presents a pMn value one order of magnitude higher than [Mn(EDTA)]$^{2-}$ and very close to that reported for [Mn(DOTA)]$^{2-}$,[22] which highlights its remarkable thermodynamic stability at physiological pH.

X-ray structure of (K(H$_2$O)$_4$){[Mn(DPAAA)(H$_2$O)]}$_2$

Slow evaporation of an aqueous solution of the [Mn(DPAAA)]$^-$ complex provided single crystals suitable for X-ray diffraction analysis. The crystals contain two [Mn(DPAAA)(H$_2$O)]$^-$ entities joined by a [K(H$_2$O)$_3$]$^+$ unit through two μ–η^1-carboxylate units (bridging Mn1 and K1) and a μ_2–η^1:η^1-carboxylate group (bridging Mn2 and K1).[23] A second potassium ion required to maintain electroneutrality could not be unequivocally

located (see the Experimental section for details). The metal ions in each [Mn(DPAAA)(H$_2$O)]$^-$ unit are directly coordinated to the amine nitrogen atom of the ligand, two pyridyl nitrogen atoms and two oxygen atoms of carboxylate groups, seven coordination being completed by the presence of a coordinated water molecule. The metal coordination environment in each [Mn(DPAAA)(H$_2$O)]$^-$ unit may be described as pentagonal bipyramidal, with the equatorial plane defined by the amine nitrogen atom and the four donor atoms of two picolinate units. An oxygen atom of the acetate pendant and a water molecule occupy the axial positions (Table 2).

Table 2. Bond distances (Å) of the Mn^{2+} coordination environments in {K(H$_2$O)$_4$}{[Mn(DPAAA)(H$_2$O)]}$_2$ [a]

Mn1–O1W	2.174(3)	Mn2–O2W	2.267(4)
Mn1–O3a	2.200(11)	Mn2–O8	2.165(3)
Mn1–N1	2.259(3)	Mn2–N3	2.249(3)
Mn1–O1	2.266(3)	Mn2–O5	2.204(3)
Mn1–N2	2.457(6)	Mn2–N4	2.475(5)

[a] See Fig. 2 for labelling.
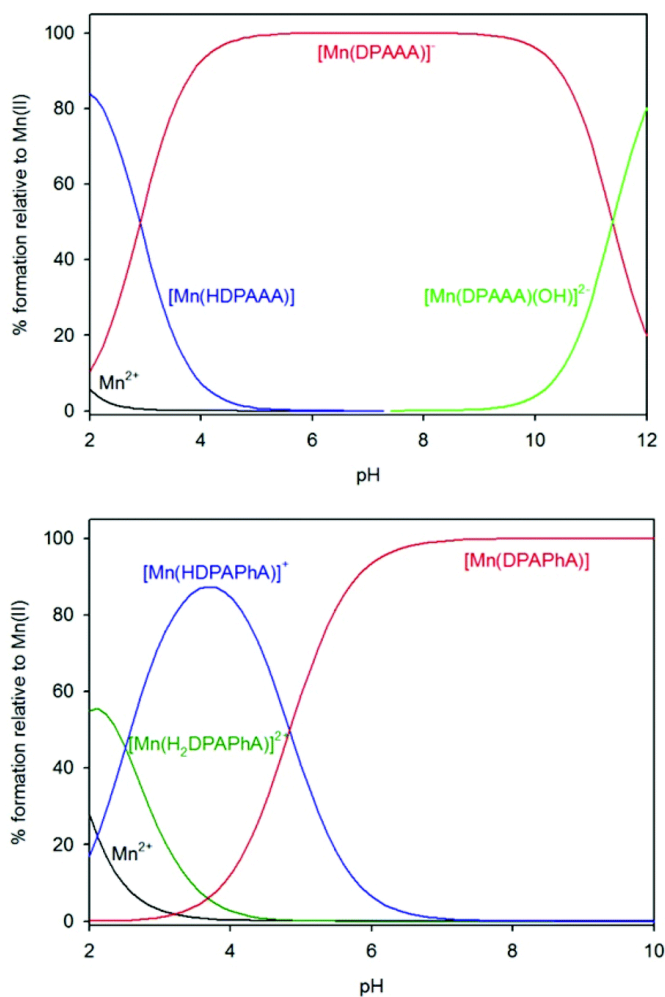
Fig. 1. Species distribution diagrams calculated for the H$_3$DPAAA:Mn^{2+} (top) and H$_2$DPAPhA:Mn^{2+} (bottom) systems. [L] = [Mn^{2+}] = 10^{-3} M.

The O3a–Mn1–O1w and O8–Mn2–O2w angles (156.7(3) and 166.11(19)°, respectively) deviate significantly from the expected values for a pentagonal bipyramidal coordination, reflecting rather distorted coordination polyhedra. The D1–Mn–D2 angles, where D1 and D2 represent adjacent donors of the equatorial plane, fall within the range 70.0–76.1°, and are therefore close to the value expected for pentagonal bipyramidal coordination (72°).

The bond distances of the Mn^{2+} coordination environments involving equivalent oxygen donor atoms in the two [Mn(DPAAA)(H$_2$O)]$^-$ entities present significant differences. For instance, the Mn1–O1 distances [2.266(3) Å] are considerably longer than the Mn2-O5 ones [2.204(3) Å], probably as a result of the μ–η^1 coordination of the carboxylate group containing O1. However, the μ_2–η^1:η^1 carboxylate coordination gives a short Mn2–O8 distance [2.165(3) Å] when compared to Mn–O3a [2.200(11) Å]. The shorter bond distance involving the carboxylate donor atom O8 results in a rather long *trans* Mn2–O2W bond [2.267(4) Å].
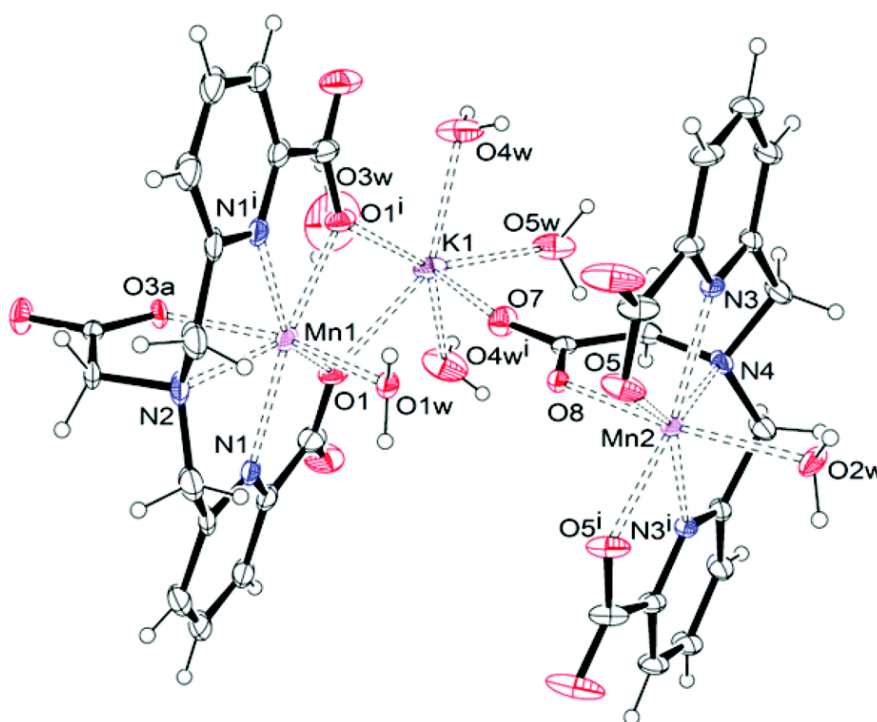
Fig. 2. View of the structure of the X-ray structure of {K(H$_2$O)$_4$}{[Mn(DPAAA)(H$_2$O)]}$_2$

<u>^{1}H NMRD and ^{17}O NMR studies of the [Mn(DPAPhA)] and [Mn(DPAAA)]$^-$ complexes</u>

Proton relaxivity, r_{1p}, which is defined as the relaxation enhancement of water protons promoted by the paramagnetic agent at 1 mM concentration, provides a convenient assessment of the efficiency of a paramagnetic complex as a contrast agent *in vitro*. The relaxivity determined for [Mn(DPAAA)]$^-$ at pH 7.4 (25 °C, 20 MHz) is 3.6 mM^{-1} s^{-1}, a value that is close to that reported for monohydrated complexes such as [Mn(EDTA)]$^{2-}$ (3.3 mM^{-1} s^{-1} at pH 7.4, 25 °C and 20 MHz). The r_{1p} value measured for [Mn(DPAPhA)] under the same conditions (6.7 mM^{-1} s^{-1}) is considerably higher, which indicates the presence of two coordinated water molecules (Fig. 3).

The relaxivity of [Mn(DPAAA)]$^-$ remains fairly constant (r_{1p} = 3.60 ± 0.15 mM^{-1} s^{-1} at 25 °C, 20 MHz) in a broad pH range from 2.5 to 11.5. Below pH 2.5, relaxivity increases due to the dissociation of the complex

and the formation of $[Mn(H_2O)_6]^{2+}$, while the slight decrease in relaxivity observed at pH > 11.5 is attributed to the formation of a hydroxo complex. Thus, the pH dependence of r_{1p} is in perfect agreement with the speciation in solution obtained from potentiometric measurements (Fig. 1).

The relaxivity of [Mn(DPAPhA)] does not change significantly in the pH range 5.9–10.2, dropping quickly at more basic pH due to the dissociation of the complex and precipitation of $Mn(OH)_2$.[24] ^{1}H relaxivity decreases from 6.7 at pH 5.9 to 6.1 at pH 3.3. This effect can be attributed to the formation of the protonated [Mn(HDPAPhA)]$^+$ species (log K_{MnLH} = 4.84(1), see above). Dissociation of the complex below pH ~ 2.7 is responsible for the slight increase in relaxivity under acidic conditions.

Proton nuclear magnetic relaxation dispersion (^{1}H NMRD) profiles of aqueous solutions [Mn(DPAPhA)] and [Mn(DPAAA)]$^-$ (Fig. 4) were recorded in the proton Larmor frequency range 0.01–70 MHz (corresponding to magnetic field strengths varying between 2.343×10^{-4} and 1.645 T). The relaxivities of both complexes decrease with increasing temperature, as expected for small chelates in which fast rotation in solution limits proton relaxivity. The NMRD profiles present a single dispersion in the range 1–10 MHz, which rules out a sizeable scalar contribution to ^{1}H relaxivity.[25,26]
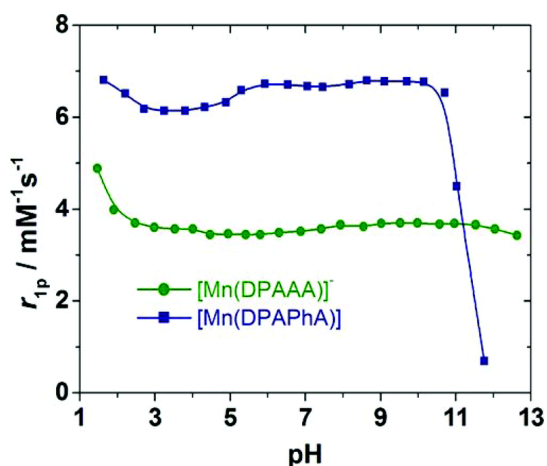

Fig. 3. Plot of the ^{1}H relaxivities (20 MHz, 25 °C) of [Mn(DPAPhA)] and [Mn(DPAAA)]$^-$ as a function of pH.
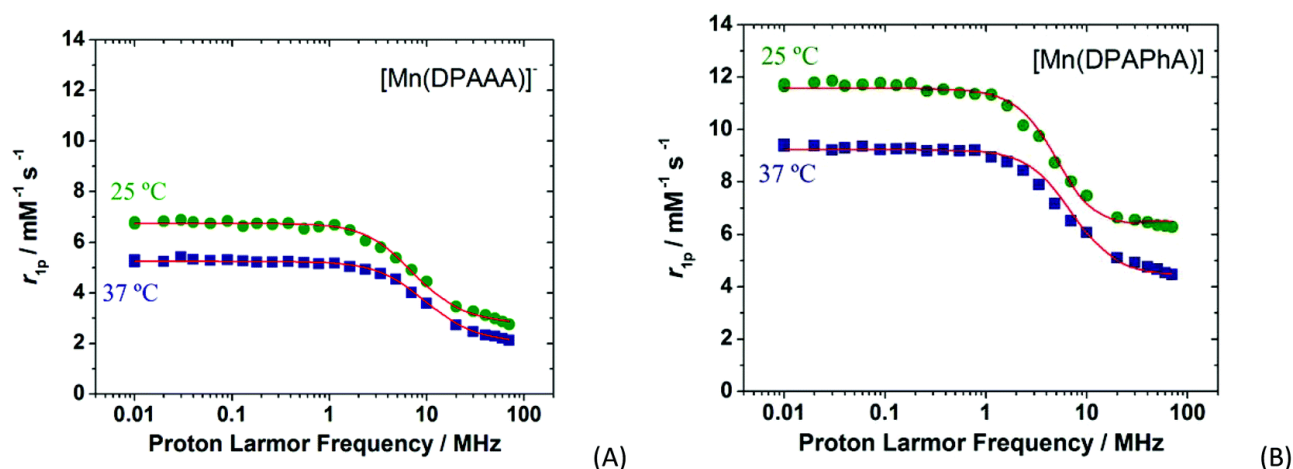
Fig. 4. ^{1}H NMRD profiles recorded at different temperatures for [Mn(DPAAA)]$^-$ and [Mn(DPAPhA)]. The lines represent the fit of the data as explained in the text.

Reduced transverse ^{17}O NMR relaxation rates of aqueous solutions of the [Mn(DPAPhA)] and [Mn(DPAAA)]⁻ complexes were recorded to gain more insight into the physicochemical parameters governing the relaxivities of these systems (Fig. 5). The $1/T_{2r}$ values increase with decreasing temperature, reach a maximum and then decrease at lower temperatures. This is typical of systems that present a changeover from a fast exchange regime at high temperatures to a slow exchange at low temperatures.[27] The lower temperature at which the maximum $1/T_{2r}$ value is observed for [Mn(DPAAA)]⁻ (*ca.* 15 °C) compared with [Mn(DPAPhA)] (~23 °C) is indicative of a somewhat faster water exchange rate in the former.
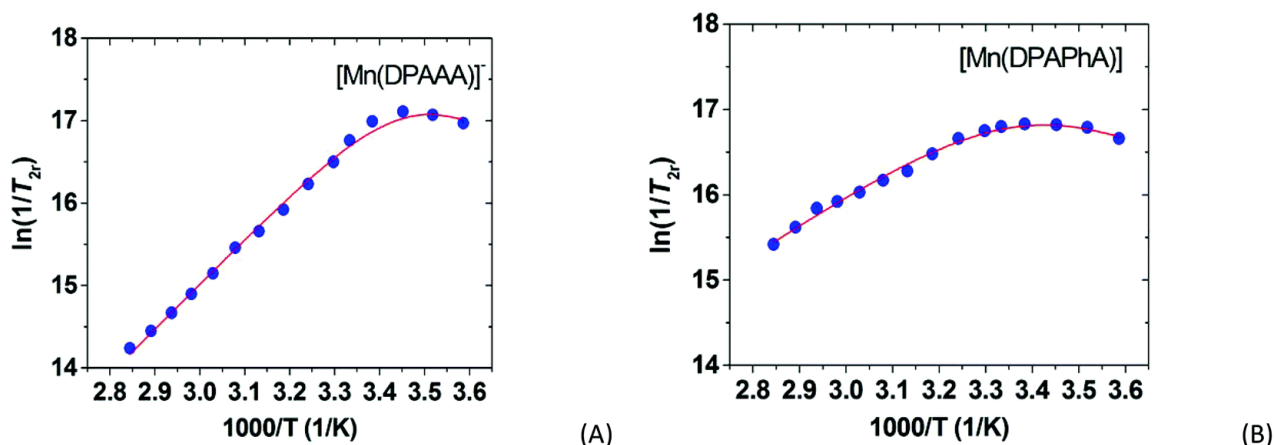

Fig. 5. Reduced transverse ^{17}O NMR relaxation rates *versus* reciprocal temperature measured for [Mn(DPAAA)]⁻ and [Mn(DPAPhA)] at 11.74 T. The lines represent the fit of the data as explained in the text.

A simultaneous fitting of the ^{1}H NMRD and ^{17}O NMR data of [Mn(DPAPhA)] and [Mn(DPAAA)]⁻ was carried out using well-established procedures.[16] Since the NMRD and ^{17}O NMR data depend on a relatively large number of parameters some of them had to be fixed during the fitting procedure to achieve a reliable analysis. The distance of closest approach for the outer-sphere contribution a_{MnH} was fixed at 3.6 Å, while the distances between the proton nuclei of the coordinated water molecules and the Mn^{2+} ion (r_{MnH}) were fixed at values corresponding to the average Mn···H distances obtained from DFT calculations (2.756 and 2.782 Å for [Mn(DPAAA)]⁻ and [Mn(DPAPhA)], respectively). The number of water molecules in the inner coordination sphere of Mn^{2+} was fixed at $q = 2$ for [Mn(DPAPhA)] and $q = 1$ for [Mn(DPAAA)]⁻. Finally, the diffusion coefficient, D^{298}_{MnH}, and its activation energy, E_{DMnH}, were fixed at the values for self-diffusion of water molecules in pure water.[28] The parameters obtained from the fittings are provided in Table 4, while the curve fits are shown in Fig. 4 and 5.

The water exchange rate determined for [Mn(DPAAA)]⁻ ($k^{298}_{ex} = 12.6 \times 10^7$ s⁻¹) is about two times that measured for [Mn(DPAPhA)] ($k^{298}_{ex} = 5.6 \times 10^7$ s⁻¹). Both complexes present lower water exchange rates than [Mn(EDTA)]²⁻,[29] approaching that determined for the aquated ion [Mn(H₂O)₆]²⁺ ($k^{298}_{ex} = 2.8 \times 10^7$ s⁻¹).[26] DFT calculations performed in aqueous solution at the TPSSh/TZVP level provide some insight into the different water exchange rates determined for [Mn(DPAPhA)] and [Mn(DPAAA)]⁻ (Fig. 6). In these calculations we included two second-sphere water molecules involved in hydrogen bonding with each coordinated water molecule, while bulk solvent effects were considered using a polarized continuum model (see Computational details below). This mixed cluster/continuum approach was shown to provide accurate Mn–O$_{water}$ distances and ^{1}H and [17]O hyperfine coupling constants of the coordinated water molecules.[9,26] The optimized geometries of the [Mn(DPAPhA)(H₂O)₂]·4H₂O and [Mn(DPAAA)(H₂O)]⁻·2H₂O systems indicate pentagonal bipyramidal coordination environments around the Mn^{2+} ion. The equatorial plane of the bipyramid is delineated by the amine nitrogen atom and the donor atoms of the picolinate units. In the case

of [Mn(DPAPhA)(H$_2$O)$_2$]·4H$_2$O two coordinated water molecules occupy the apical positions, while for [Mn(DPAAA)(H$_2$O)]$^-$·2H$_2$O the apical positions contain a coordinated water molecule and an oxygen atom of the acetate group of the ligand.
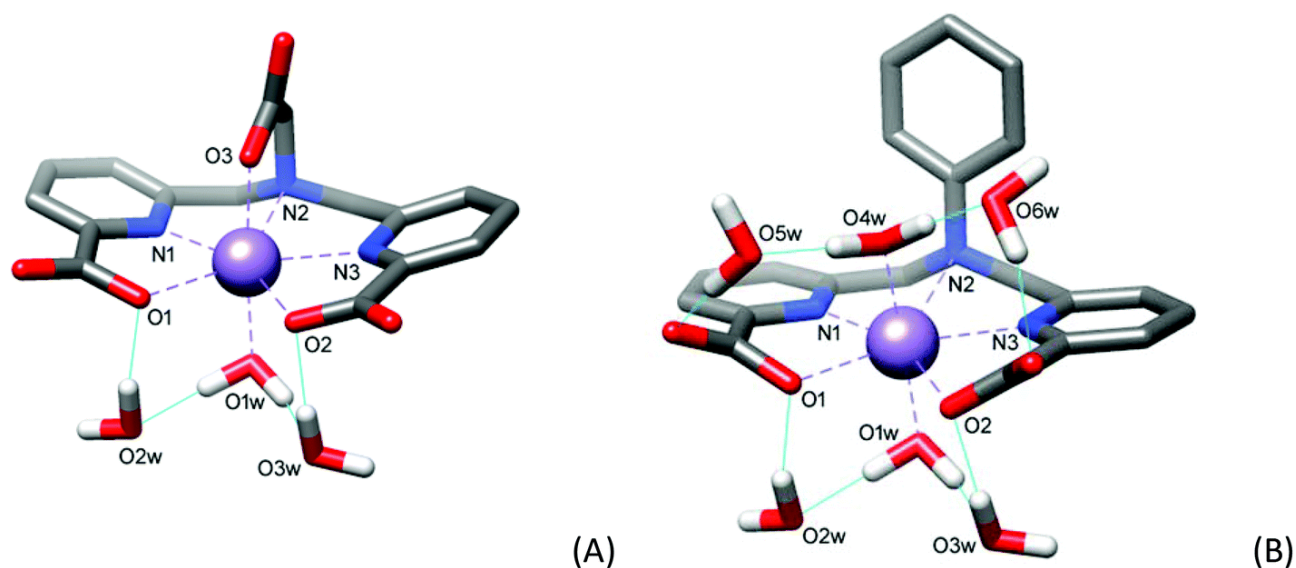
Fig. 6. Structures of the [Mn(DPAAA)(H$_2$O)]$^-$·2H$_2$O and [Mn(DPAPhA)(H$_2$O)$_2$]·4H$_2$O systems obtained with DFT calculations (TPSSh/TZVP). Calculated bond distances (Å): [Mn(DPAAA)(H$_2$O)]$^-$·2H$_2$O, Mn–N(1), 2.314; Mn–N(2), 2.521; Mn–N(3), 2.316; Mn–O(1), 2.289; Mn–O(2), 2.291; Mn–O(1w), 2.288; Mn–O(3), 2.131. [Mn(DPAPhA)(H$_2$O)$_2$]·4H$_2$O, Mn–N(1), 2.285; Mn–N(2), 2.885; Mn–N(3), 2.268; Mn–O(1), 2.225; Mn–O(2), 2.289; Mn–O(1w), 2.250; Mn–O(4w), 2.237.

The calculated Mn–O$_{water}$ distances involving the coordinated water molecule(s) are 2.288 Å for [Mn(DPAAA)(H$_2$O)]$^-$·2H$_2$O and 2.237 and 2.250 Å for [Mn(DPAPhA)(H$_2$O)$_2$]·4H$_2$O. Thus, the Mn–O$_{water}$ distance in [Mn(DPAAA)(H$_2$O)]$^-$ is significantly longer than those of the complex with DPAPhA^{2-}, revealing weaker binding of the coordinated water molecule in the former. Water exchange in these seven-coordinated complexes is expected to follow a dissociatively activated mechanism, the rate determining step being the rupture of the Mn–O$_{water}$ bond to give a six-coordinated transition state. Thus, the stronger the Mn–O$_{water}$ bond, the slower the water exchange process is expected to be. Similar trends correlating the strength of the Gd–O$_{water}$ bonds and the corresponding water exchange rates were observed for nine-coordinate Gd^{3+} complexes undergoing dissociatively activated water exchange processes.[30]

The values obtained for the ^{17}O hyperfine coupling constants are in the lower part of the range typically observed for Mn^{2+} complexes ($A_O/\hbar = 25 \times 10^6$ to 47×10^6 rad s^{-1}), being very similar to the values reported for [Mn(H$_2$O)$_6$]$^{2+}$ and other small complexes.[31] Concerning the parameters related to the electron spin relaxation of the metal ion (the electronic correlation time for the modulation of the zero-field-splitting interaction, τ_V, and the mean square zero-field-splitting energy, Δ^2), the parameters obtained from the analysis of NMRD and ^{17}O NMR data are similar to those obtained for other Mn^{2+} complexes (Table 3).

Characterization of the lipophilic derivatives [Mn(DPAC6PhA)] and [Mn(DPAC12A)]

The critical micelle concentration (cmc) of [Mn(DPAC6PhA)] and [Mn(DPAC12A)] was investigated by using relaxometric measurements at 20 MHz and 25 °C.[32] The paramagnetic relaxation enhancement of water proton nuclei (R^{obs}_1) increased linearly with the concentration of the [Mn(DPAC6PhA)] complex in the range 0.07–0.61 mM (Fig. S17, ESI†). The slope of the linear plot provides a relaxivity of the non-

aggregated form of 4.1 mM^{-1} s^{-1}. This value is consistent with that obtained from NMRD studies, which confirms the lack of self-aggregation of the complex under these conditions (Fig. S18, ESI†). Precipitation of the complex was observed at higher concentrations, thus preventing cmc determination. Surprisingly, the relaxivity determined for [Mn(DPAC6PhA)] is considerably lower than that of the bis-hydrated [Mn(DPAPhA)] complex (6.6 mM^{-1} s^{-1}), which suggests that the introduction of the hexyl chain into the ligand scaffold lowers the hydration number of the complex.

Table 3. Parameters obtained from the simultaneous analysis of ^{17}O NMR and ^{1}H NMRD data[a]

	[Mn(DPAAA)]$^-$	[Mn(DPAPhA)]	[Mn(DPAMeA)][b]	[Mn(EDTA)]$^{2-}$ [c]	[Mn(H$_2$O)$_6$]$^{2+}$ [d]
r_{1p} at 25/37 °C/mM^{-1} s^{-1b}	3.5/2.7	6.6/5.1	5.3/4.2	3.3/2.8	
k^{298}_{ex}/10^7 s^{-1}	12.6 ± 0.5	5.6 ± 0.6	30.6	47.1	2.82
$\Delta H^{\ddagger}$/kJ mol^{-1}	42.7 ± 1.0	27.2 ± 2.3	28.1	33.5	45.6
τ^{298}_{R}/ps	47.6 ± 0.2	81.0 ± 0.5	47.8	57	30.0
E_r/kJ mol^{-1}	22.8 ± 0.4	27.0 ± 2.6	25.3	21.8	16.7
τ^{298}_{V}/ps	19.4 ± 0.2	15.6 ± 0.1	39.2	27.9	10.0
E_v/kJ mol^{-1}	1.0^a	1.0^a	1.0^a	1.0^a	14.6
D^{298}_{MnH}/10^{-10}m^2 s^{-1}	22.4^a	22.4^a	22.4^a	23.1	23.0^a
E_{DMnH}/kJ mol^{-1}	17.3^a	17.3^a	17.3^a	18.9	29.7
Δ^2/10^{19} s^{-2}	5.5 ± 0.2	11.5 ± 0.4	2.38	6.9	0.6
$A_O/\hbar$/10^6 rad s^{-1}	−31.5 ± 0.6	−25.0 ± 0.6	−45.8	−40.5	−34.6
r_{MnH}/Å	2.756^a	2.782^a	2.74^a	2.83^a	2.83
a_{MnH}/Å	3.6^a	3.6^a	3.6^a	3.6^a	3.6
q^{298}	1^a	2^a	2^a	1^a	6

^{a} Parameters fixed during the fitting procedure. ^{b} Data from ref. 16. ^{c} Data from ref. 29. ^{d} Data from ref. 26.

The R^{obs}_1 values measured from solutions of [Mn(DPAC12A)] present two linear ranges with an inflection point at a complex concentration of ~0.1 mM (Fig. S19, ESI†). The analysis of the data provides a cmc of 96(9) μM with relaxivity values of r_{1p} = 5.3 mM^{-1} s^{-1} and r_{1p} = 8.5 mM^{-1} s^{-1} for the non-aggregated and aggregated forms, respectively. The cmc determined for [Mn(DPAC12A)] is similar to that reported for a charge neutral Eu^{3+} complex having a C$_{12}$ alkyl chain (67 μM),[33] but considerably lower than that determined for a similar system having negatively charged hydrophilic head units (4.5 mM).[34] These results suggest that repulsive electrostatic interactions among the negatively charged head units are detrimental to the formation of micelles.

The relaxivity of [Mn(DPAC12A)] below the cmc (r_{1p} = 5.3 mM^{-1} s^{-1}) is lower than that of [Mn(DPAMeA)], which suggests that the incorporation of the C$_{12}$ alkyl chains into the ligand skeleton lowers the hydration number of the complex. As expected, the NMRD profile recorded below the cmc is typical of a small Mn^{2+} complex (Fig. 7). The best-fit analysis confirms these qualitative observations. The NMRD profile below cmc is well reproduced by fixing at one the number of inner-sphere water molecules, at a distance of 2.782 Å and with a residence lifetime of 10 ns (298 K). The relaxivity is limited by the rotational dynamics even though the parameter τ_R assumes a value of 123 ps, more than two times that of [Mn(EDTA)]$^-$ and [Mn(DPAAA)]$^-$. The longer τ_R reflects the presence of the pendant aliphatic chain and its effect is apparent from the nearly vanished field-dependence of relaxivity at high frequencies. The electronic relaxation parameters assume typical values: τ_V = 21.4 ps and Δ^2 = 8.1 × 10^{19} s^{-2}. Conversely, above the cmc the NMRD profile presents a pronounced peak around 30 MHz that is characteristic of slowly tumbling

systems. The NMRD at high field (>3 MHz) was fitted using the Lipari–Szabo approach, which separates the global and local motions of the system.[35] The analysis was performed by using as adjustable parameters those describing electron spin relaxation (τ_v and Δ^2), the correlation times describing global (τ_{RG}) and local (τ_{RL}) motions and the generalized order parameter S^2, which takes a value of 0 if the internal motion is isotropic and a value of $S^2 = 1$ if the motion is completely restricted. The hydration number was fixed at $q = 1$, while the Mn$\cdots$H distance (2.74 Å), the distance of closest approach of a second-sphere water molecule ($a_{MnH} = 3.6$ Å) and the diffusion coefficient ($D^{298}_{MnH} = 2.24 \times 10^{-10}$ m^2 s^{-1}) were fixed at reasonable values (Table 3). The results of the fit provided $\tau_{RG} = 5$ ns and $\tau_{RL} = 95$ ps, with $S^2 = 0.27$, indicating that relaxivity is limited by local rotational flexibility (Table 4).[36] Analysis of the NMRD profile recorded at 37 °C provides very similar results (Fig. S20, ESI†). ^{1}H relaxivity decreases with increasing temperature, which indicates that the exchange rate of the coordinated water molecule is not limiting r_{1p}.

Table 4. Selected parameters obtained from the analysis of the NMRD profiles using the Lipari–Szabo approach (25 °C)

	Mn(DPAC12A)[a]	Mn(DPAC12A) + HSA[b]	Mn(DPAC6PhA) + HSA[c]
r_{1p} (20 MHz)	8.5 ± 0.1	15.5 ± 0.3	45.5 ± 1.4
τ_{RG} (ns)	5.5 ± 0.7	50 (fixed)	50 (fixed)
τ_{RL} (ps)	91 ± 3	306 ± 10	1235 ± 52
S^2	0.27 ± 0.01	0.26 ± 0.01	0.43 ± 0.02
K_A/M^{-1}	—	$1.3 \pm 0.4 \times 10^5$	$7.1 \pm 0.1 \times 10^3$

[a] $\tau_v = 49 \pm 8$ ps; $\Delta^2 = 5.4 \pm 0.6$ s^{-2}. [b] $\tau_v = 22 \pm 9$ ps; $\Delta^2 = 1.0 \pm 0.6$ s^{-2}. [c] $\tau_v = 18 \pm 8$ ps; $\Delta^2 = 0.84 \pm 0.04$ s^{-2}.
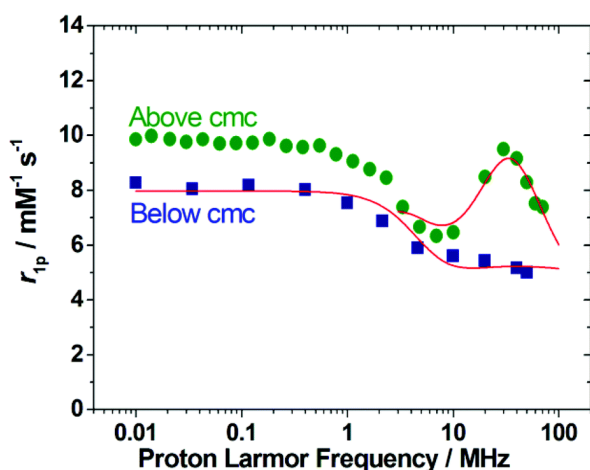
Fig. 7. ^{1}H NMRD profiles recorded at 25 °C for [Mn(DPAC12A)] above and below the cmc. The red lines represent the fit of the data as described in the text.

Interaction of the lipophilic derivatives [Mn(DPAC6PhA)] and [Mn(DPAC12A)] with HSA

The interaction of [Mn(DPAC6PhA)] and [Mn(DPAC12A)] with HSA was investigated by measuring the R^{obs}_1 values of a diluted solution of the complex as a function of protein concentration at a fixed frequency and temperature. R^{obs}_1 increases with the concentration of the protein because of the increase in the fraction of bound complexes that is characterized by a slower reorientational motion. The analysis of the

titration data (fitted to a 1 : 1 binding isotherm) affords the association constant K_A, the number of equivalent and independent binding sites n (assumed to be 1) and the relaxivity of the bound form. The titration profile obtained for [Mn(DPAC6PhA)] presents a rather sharp inflection point, which is indicative of a rather high stability constant (Fig. 8). On the contrary, [Mn(DPAC12A)] provides a smooth titration profile, characteristic of a smaller association constant. Inspection of the titration profiles also shows that the relaxivity of the bound form is considerably higher in the case of [Mn(DPAC6PhA)]. The fit of the data confirms these qualitative observations (Table 4). The association constant determined for [Mn(DPAC12A)] $(1.3 \times 10^5 \, M^{-1})$ is 1–2 orders of magnitude higher than those determined for Mn^{2+} complexes containing benzyloxymethyl groups,[37] and *ca.* 18 times higher than that obtained for [Mn(DPAC6PhA)]. These results suggest that a lipophilic C_{12} alkyl chain provides a stronger interaction with the protein than benzyloxymethyl and 4-hexylphenyl moieties. This could be related to a better ability to penetrate inside the hydrophobic binding cavity of HSA.[38]
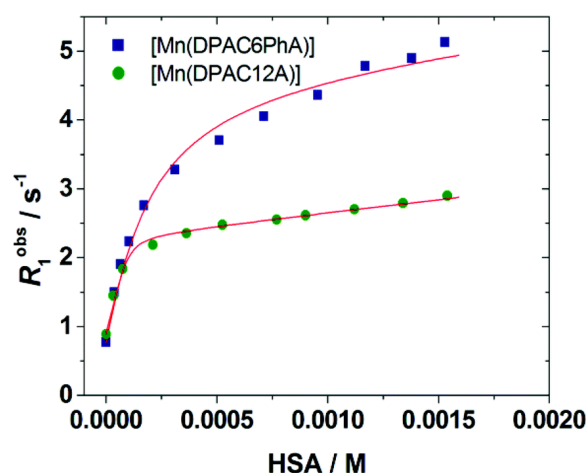
Fig. 8. Changes in the observed longitudinal relaxation rates of water protons observed upon the addition of HSA to solutions of the lipophilic [Mn(DPAC6PhA)] (0.094 mM) and [Mn(DPAC12A)] (0.098 mM) complexes (25 °C). The red lines represent the fit of the data to a 1 : 1 binding isotherm.
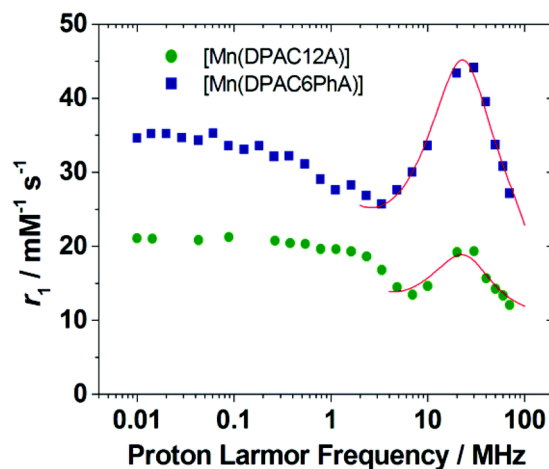
Fig. 9. ^{1}H NMRD profiles obtained at 25 °C for the adducts formed by [Mn(DPAC12A)] and [Mn(DPAC6PhA)] with HSA. The red lines represent the fit of the data above cmc using the Lipari–Szabo approach.

The NMRD profiles recorded for the [Mn(DPAC6PhA)] and [Mn(DPAC12A)] complexes fully bound to HSA (Fig. 9) are characteristic of slowly tumbling species. The relaxivity of [Mn(DPAC6PhA)] at *ca.* 20 MHz and 25 °C (45.5 mM^{-1} s^{-1}) is close to those observed for HSA adducts of Mn^{2+} complexes containing benzyloxymethyl groups, while the relaxivity of [Mn(DPAC12A)] under the same conditions is clearly lower (15.5 mM^{-1} s^{-1}). The analyses of the NMRD profiles using the Lipari–Szabo model (Table 4) clearly indicate that an increased local flexibility is responsible for the lower relaxivity of the adduct formed between [Mn(DPAC12A)] and HSA, as demonstrated by the lower values of τ_{RL} and S^2. Thus, the alkyl C$_{12}$ chain provides strong interactions with the protein, but its flexibility prevents attaining high relaxivities.

Conclusions

We have designed a series of pentadentate or hexadentate ligands that contain a pentadentate 6,6′-(azanediylbis(methylene))dipicolinic acid binding motif that can be easily functionalised with groups containing additional donor atoms or lipophilic chains. The syntheses of the ligands followed a straightforward approach that allowed developing the versatile family of picolinate ligands for Mn^{2+} complexation.

The pentadentate DPAPhA^{2-} and DPAMeA^{2-} ligands give rise to bis-aquated Mn^{2+} complexes in solution. The high hydration state of these complexes is associated with enhanced relaxivity values, fully comparable with those measured for $q = 2$ Gd^{3+} complexes such as GdDO3A and GdPCTA.[4] Clearly, the higher magnetic moment of Gd^{3+} is offset by the shorter Mn–Hw distance of the bound water molecule(s). Therefore, as regards the efficiency as relaxation agents, the Mn^{2+} complexes with picolinate ligands are virtually equivalent to the Gd^{3+} chelates. The functionalized derivatives with lipophilic chains can self-aggregate to form micelles. They are also able to form rather stable adducts with HSA, particularly when incorporating a flexible dodecyl chain. However, the relaxivity of the bound form is partially quenched due to the contribution of local motions arising from the rotational flexibility of the binding unit. An intriguing result obtained in this study is the likely reduction of the hydration number upon incorporating aliphatic chains into the ligand scaffold.

The present contribution extends the number of Mn^{2+} systems that have been characterised in the context of MRI contrast agents as an alternative to the classical Gd^{3+} complexes. We have shown that the relaxivities of Mn^{2+} complexes can be modulated by changing the hydration number or by introducing lipophilic units into the ligand scaffold, very much like what is observed in the case of Gd^{3+} complexes. The relaxivities of the adducts formed with HSA are also comparable to those attained with lipophilic Gd^{3+} agents. However, the Mn^{2+} complexes with the pentadentate ligands lack sufficient stability for use *in vivo*. These results confirm the difficulty of developing Mn-based $q = 2$ complexes with a sufficient stability and kinetic inertness to be employed in clinical diagnostics.

On the other hand, the hexadentate ligand DPAAA^{3-} forms with Mn^{2+} a complex with stability and relaxivity quite comparable to those of [Mn(EDTA)]$^{2-}$. Of particular interest is the remarkable thermodynamic stability of [Mn(DPAAA)]$^{-}$ at physiological pH, evidenced by the pM value of 8.98, similar to that of [Mn(DOTA)]$^{2-}$ (Scheme 1). This complex has a relaxivity significantly greater than that of [Mn(1,4-DO2A)] as the latter shows in solution a small population (10%) of a six-coordinate isomeric form ($q = 0$).[29] Moreover, when compared with the $q = 1$ [Mn(NOMPA)]$^{+}$ complex, it shows a similar relaxivity but a stability constant increased by almost 3 log K units.[9a]

Despite these interesting and encouraging results, there is still a need to expand the available library of Mn-based chelates so far investigated to achieve better and more reliable information on the correlation between solution structure and molecular relaxation parameters. Moreover, it is very important to obtain accurate

information relating to the thermodynamic stability and kinetic inertness of the complexes. This is key to develop safer probes with enhanced efficacy (relaxivity) for *in vivo* use.

Experimental section

Materials and methods

All reagents and solvents were commercially available and used without further purification. SiO_2 (Fluka, pore size 60 Å, 70–230 mesh) was used for preparative column chromatography. ^1H and ^{13}C NMR spectra were recorded at 25 °C on Bruker Avance 300 MHz and Bruker Avance 500 MHz spectrometers. High resolution ESI-TOF mass spectra were recorded using a LC-Q-q-TOF (Applied Biosystems QSTAR Elite) spectrometer in the positive mode. Elemental analyses were carried out using a ThermoQuest Flash EA 1112 elemental analyser. IR spectra were recorded using a Bruker Vector 22 spectrophotometer equipped with a Golden Gate attenuated total reflectance (ATR) accessory (Specac).

Synthesis of 6,6′-((dodecylazanediyl)bis(methylene))dipicolinic acid (H₂DPAC12A)

6-Chloromethylpyridine-2-carboxylic acid ethyl ester (1.18 g, 5.91 mmol) and K_2CO_3 (1.25 g, 9.05 mmol) were added to a solution of dodecylamine (0.51 g, 2.75 mmol) in 50 mL of acetonitrile. The mixture was stirred for a period of 3 days at room temperature and, after this, heated to 60 °C for 4 days. The excess K_2CO_3 was filtered off, the filtrate was concentrated to dryness, and the yellow residue was extracted with 50 mL of a H_2O and $CHCl_3$ (1 : 3) mixture. The organic phase was evaporated to dryness to give an oily residue that was purified by column chromatography on SiO_2 with a $CHCl_3$/MeOH 2% mixture as the eluent to give the ester precursor (0.984 g, 1.92 mmol) as a yellow oil in 70% yield. ^1H NMR (CDCl₃, 300 MHz, 25 °C, TMS): δ 7.96 (m, 2H), 7.79 (m, 4H), 4.45 (c, 4H, ^3J = 7.2 Hz), 3.92 (s, 4H), 2.54 (m, 2H), 1.52 (m, 2H), 1.42 (t, 6H, ^3J = 7.2 Hz), 1.22 (m, 17H), 0.87 ppm (m, 4H). ^{13}C NMR (CDCl₃, 75 MHz, 25 °C, TMS): δ 166.3, 160.9, 147.6, 137.1, 125.6, 123.3, 61.8, 60.3, 54.7, 31.9, 29.6 (4 C), 29.5, 29.3, 27.3, 27.2, 22.7, 14.3, 14.1 ppm. ESI⁺/HR-MS (CH₃CN): m/z 512.3478; calcd for $[C_{30}H_{46}N_3O_4]^+$ 512.3482. IR (ATR): v 1741 and 1716 cm⁻¹ (C=O).

A solution of ester precursor (0.984 g, 1.92 mmol) in 6 M HCl (20 mL) was heated to reflux for 3 h, resulting in the precipitation of an abundant white solid. It was collected by filtration and dried *in vacuo* to give H₂DPAC12A (0.803 g) in 85% yield. ^1H NMR (D₂O, pD 7.0, 500 MHz, 25 °C, TMS): δ 7.62 (m, 4H), 7.26 (m, 2H), 4.29 (m, 4H), 2.95 (m, 2H), 1.59–0.74 ppm (m, 23H). ^{13}C NMR (D₂O, pD 7.0, 125.8 MHz, 25 °C, TMS): δ 171.2, 153.2, 151.6, 138.2, 125.5, 123.5, 58.7, 55.6, 31.9, 29.8, 29.7, 29.6, 29.5, 29.4, 29.1, 26.7, 24.2, 22.6, 13.9 ppm. ESI⁺/MS (CH₃CN): m/z 456 ($[C_{26}H_{38}N_3O_4]^+$). IR (ATR): v 1733 cm⁻¹ (C=O). Anal. calcd for $C_{26}H_{37}N_3O_4 \cdot HCl$: C, 63.46; H, 7.78; N, 8.54. Found: C, 63.40; H, 7.52; N, 8.23%.

Synthesis of 6,6′-(((carboxymethyl)azanediyl)bis(methylene))dipicolinic acid (H₃DPAAA)

6-Chloromethylpyridine-2-carboxylic acid ethyl ester (1.18 g, 5.91 mmol) and K_2CO_3 (1.64 g, 11.8 mmol) were added to a solution of glycinamide hydrochloride (0.304 g, 2.75 mmol) in 50 mL of acetonitrile. The mixture was stirred for a period of 3 days at room temperature and, after this, heated to 60 °C for 4 days. The excess K_2CO_3 was filtered off, the filtrate was concentrated to dryness, and the yellow residue was extracted with 50 mL of a H_2O and $CHCl_3$ (1 : 3) mixture. The organic phase was evaporated to dryness to give an oily residue that was purified by column chromatography on SiO_2 with a $CHCl_3$/MeOH 5% mixture as the eluent to give the ester precursor (0.750 g, 1.87 mmol) as a pale yellow oil in 68% yield. ^1H NMR (CDCl₃, 300 MHz, 25 °C, TMS): δ 9.40 (s, 1H), 7.79 (m, 4H), 7.98 (d, 2H, ^3J = 7.7 Hz), 7.74 (t, 2H, ^3J = 7.7 Hz), 7.53 (d, 2H, ^3J = 7.7 Hz), 5.67 (s, 1H), 4.46 (c, 4H, ^3J = 7.2 Hz), 4.00 (s, 4H), 3.38 (s, 2H), 1.44 ppm (t, 6H, ^3J = 7.2 Hz). ^{13}C NMR (CDCl₃, 75 MHz, 25 °C, TMS): δ 174.6, 165.0, 158.9, 147.7, 137.5, 126.3, 123.7, 61.8, 60.0,

58.4, 14.3 ppm. ESI$^+$/HR-MS (CH$_3$CN): m/z 401.1825; calcd for [C$_{20}$H$_{25}$N$_4$O$_5$]$^+$ 401.1819. IR (ATR): ν 1716 and 1673 cm^{-1} (C=O).

A solution of the ester precursor (0.750 g, 1.87 mmol) in 6 M HCl (20 mL) was heated to reflux for 6 h, and then the solvent was removed using a rotary evaporator to give a yellow oil. A small amount of H$_2$O was added (∼20 mL) and the mixture was evaporated to dryness. This process was repeated twice with addition of H$_2$O and twice with addition of diethyl ether (∼20 mL) to give H$_3$DPAAA (0.675 g) as a pale yellow solid in 83% yield. ^{1}H NMR (D$_2$O, pD 7.0, 500 MHz, 25 °C, TMS): δ 7.67 (t, 2H, ^3J = 7.7 Hz), 7.63 (d, 2H, ^3J = 7.7 Hz), 7.34 (d, 2H, ^3J = 7.7 Hz), 4.25 (s, 4H), 3.61 ppm (m, 2H). ^{13}C NMR (D$_2$O, pD 7.0, 125.8 MHz, 25 °C, TMS): δ 174.5, 172.2, 153.1, 152.6, 138.5, 126.3, 123.1, 59.6, 58.6 ppm. ESI$^+$/MS (CH$_3$CN): m/z 346 ([C$_{16}$H$_{16}$N$_3$O$_6$]$^+$). IR (ATR): ν 1769 and 1749 cm^{-1} (C=O). Anal. calcd for C$_{16}$H$_{15}$N$_3$O$_6$·2HCl·H$_2$O: C, 44.05; H, 4.39; N, 9.63. Found: C, 44.29; H, 4.25; N, 9.73%.

Synthesis of 6,6′-((phenylazanediyl)bis(methylene))dipicolinic acid (H$_2$DPAPhA)

6-Chloromethylpyridine-2-carboxylic acid ethyl ester (1.97 g, 9.86 mmol) and K$_2$CO$_3$ (2.08 g, 15.1 mmol) were added to a solution of aniline (0.424 g, 4.55 mmol). The mixture was heated to 60 °C for 5 days and after this a catalytic amount of KI was added and the mixture was refluxed for a period of 2 days. The excess K$_2$CO$_3$ was filtered off, the filtrate was concentrated to dryness, and the yellow residue was extracted with 50 mL of a H$_2$O and CHCl$_3$ (1 : 3) mixture. The organic phase was evaporated to dryness to give an oily residue that was purified by column chromatography on SiO$_2$ with a CHCl$_3$/MeOH 2% mixture as the eluent to give the ester precursor (1.24 g, 2.95 mmol) as a yellow oil in 65% yield. ^{1}H NMR (CDCl$_3$, 300 MHz, 25 °C, TMS): δ 8.01 (d, 2H, ^3J = 7.7 Hz), 7.78 (t, 2H, ^3J = 7.7 Hz), 7.46 (d, 2H, ^3J = 7.7 Hz), 7.18 (m, 2H), 6.72 (m, 3H), 4.94 (s, 4H), 4.49 (c, 4H, ^3J = 7.2 Hz), 1.44 ppm (t, 6H, ^3J = 7.2 Hz). ^{13}C NMR (CDCl$_3$, 75 MHz, 25 °C, TMS): δ 165.1, 159.5, 148.4, 148.0, 137.8, 129.4, 123.8, 123.5, 117.6, 112.4, 61.9, 51.2, 14.3 ppm. ESI$^+$/HR-MS (CH$_3$CN): m/z 420.1918; calcd for [C$_{24}$H$_{26}$N$_3$O$_4$]$^+$ 420.1917. IR (ATR): ν 1716 cm^{-1} (C=O).

A solution of ester precursor (1.24 g, 2.95 mmol) in 6 M HCl (20 mL) was heated to reflux for 24 h, and then the solvent was removed in a rotary evaporator to give a brown oil. A small amount of H$_2$O was added (∼20 mL) and the mixture evaporated to dryness. This process was repeated twice with addition of H$_2$O and twice with addition of diethyl ether (∼20 mL) to give H$_2$DPAPhA (1.24 g) as a dark brown solid in 80% yield. ^{1}H NMR (D$_2$O, pD 7.0, 300 MHz, 25 °C, TMS): δ 7.70 (m, 4H), 7.30 (d, 2H, ^3J= 6.9 Hz), 7.09 (m, 2H), 6.65 (m, 3H), 4.82 ppm (s, 4H). ^{13}C NMR (D$_2$O, pD 7.0, 75 MHz, 25 °C, TMS): δ 172.9, 158.3, 153.4, 147.7, 129.6, 122.9, 122.1, 117.5, 114.4, 112.9, 56.6 ppm. ESI$^+$/MS (CH$_3$CN): m/z 364 ([C$_{20}$H$_{18}$N$_3$O$_4$]$^+$). IR (ATR): ν 1731 cm^{-1} (C=O). Anal. calcd for C$_{20}$H$_{17}$N$_3$O$_4$·4HCl·H$_2$O: C, 45.56; H, 4.40; N, 7.07. Found: C, 46.02; H, 4.50; N, 7.04%.

Synthesis of 6,6′-(((4-hexylphenyl)azanediyl)bis(methylene))dipicolinic acid (H$_2$DPAC6PhA)

6-Chloromethylpyridine-2-carboxylic acid ethyl ester (2.03 g, 10.2 mmol) and K$_2$CO$_3$ (2.14 g, 15.5 mmol) were added to a solution of 4-hexylaniline (0.833 g, 4.70 mmol). The mixture was heated to 60 °C for 5 days and after this a catalytic amount of KI was added and the mixture was refluxed for a period of 2 days. The excess K$_2$CO$_3$ was filtered off, the filtrate was concentrated to dryness, and the yellow residue was extracted with 50 mL of a H$_2$O and CHCl$_3$ (1 : 3) mixture. The organic phase was evaporated to dryness to give an oily residue that was purified by column chromatography on SiO$_2$ with a CHCl$_3$/MeOH 2% mixture as the eluent to give the ester precursor (1.70 g, 3.38 mmol) as a yellow oil in 72% yield. ^{1}H NMR (CDCl$_3$, 500 MHz, 25 °C, TMS): δ 8.00 (d, 2H, ^3J = 7.8 Hz), 7.77 (t, 2H, ^3J = 7.8 Hz), 7.47 (d, 2H, ^3J = 7.8 Hz), 6.99 (d, 2H, ^3J = 8.7 Hz), 6.61 (d, 2H, ^3J = 8.7 Hz), 4.91 (s, 4H), 4.49 (c, 4H, ^3J = 7.2 Hz), 2.47 (m, 2H), 1.54 (m, 2H), 1.44 (t, 6H, ^3J = 7.2 Hz), 1.28 (m, 6H), 0.87 ppm (m, 3H). ^{13}C NMR (CDCl$_3$, 125.5 MHz, 25 °C, TMS): δ 165.1, 159.8, 148.3, 145.8, 137.8, 132.1, 129.3, 123.9, 123.5, 112.4, 61.9, 57.3, 34.8, 31.7, 31.6, 29.0, 22.6, 14.3,

14.1 ppm. ESI$^+$/HR-MS (CH$_3$CN): m/z 504.2861; calcd for [C$_{30}$H$_{38}$N$_3$O$_4$]$^+$ 504.2856. IR (ATR): v 1738 and 1717 cm^{-1} (C=O).

A solution of the ester precursor (1.70 g, 3.38 mmol) in 6 M HCl (20 mL) was heated to reflux for 24 h, and then the solvent was removed in a rotary evaporator to give a yellow oil. A small amount of H$_2$O was added (~20 mL) and the mixture evaporated to dryness. This process was repeated twice with addition of H$_2$O and twice with addition of diethyl ether (~20 mL) to give H$_2$DPAC6PhA (1.96 g) as a pale brown solid in 85% yield. ^{1}H NMR (D$_2$O, pD 7.0, 500 MHz, 25 °C, TMS): δ 7.47 (m, 2H), 7.05 (m, 2H), 6.74 (m, 2H), 6.48 (m, 2H), 6.27 (m, 2H), 4.56 (s, 4H), 2.06 (m, 2H), 1.16–0.90 (m, 8H), 0.56 ppm (m, 3H). ^{13}C NMR (D$_2$O, pD 7.0, 125.8 MHz, 25 °C, TMS): δ 171.3, 157.8, 152.7, 145.7, 138.4, 131.0, 129.0, 122.4, 112.5, 56.1, 34.5, 31.5, 31.3, 28.9, 22.4, 13.7 ppm. ESI$^+$/MS (CH$_3$CN): m/z 448 ([C$_{26}$H$_{30}$N$_3$O$_4$]$^+$). IR (ATR): v 1682 cm^{-1} (C=O). Anal. calcd for C$_{26}$H$_{29}$N$_3$O$_4$·6HCl·H$_2$O: C, 45.63; H, 5.45; N, 6.14. Found: C, 45.65; H, 5.43; N, 5.75%.

Equilibrium measurements

All the equilibrium measurements were conducted at a constant ionic strength maintained by 0.15 M NaCl at 298 K. The protonation constants of the DPAAA^{3-} and DPAPhA^{2-} ligands were determined by pH-potentiometric titrations using 0.002 M ligand solutions (8 mL) and a standardised 0.2 M NaOH solution as the titrant. The stability and protonation constants of Mn^{2+}complexes were also determined by pH-potentiometric titrations using 1 : 1 metal to ligand concentration ratios. Equilibrium constants were calculated using base mL–pH data pairs obtained in the pH range 1.7–12.0. The pH-potentiometric titrations were carried out using a 785 DMP Titrino titration workstation equipped with a Metrohm-6.0233.100 combined electrode. The samples were stirred during the titrations while N$_2$ gas was bubbled through the solutions to avoid CO$_2$. For the calibration of the pH meter, KH-phthalate (pH = 4.002) and borax (pH = 8.970) buffers were used. The H$^+$ concentration was obtained from the measured pH values using the method proposed by Irving $et\ al.$[39] A 0.01 M HCl (0.15 M NaCl) solution was titrated with 0.2 M NaOH and the differences between the measured and calculated pH values were used to calculate [H$^+$] from the pH values determined in the titration experiments. Equilibrium constants were calculated with the PSEQUAD program.[40]

^{1}H NMRD and ^{17}O NMR measurements

The Mn^{2+} complexes have been prepared by mixing solutions of MnCl$_2$ and the ligand (in $ca.$ 5% molar excess) and adjusting the pH to 7.4 with HCl or NaOH. The exact concentration of the aqueous solutions for ^{1}H NMRD and ^{17}O NMR measurements was determined by the BMS shift method at 11.7 T.[41] The proton $1/T_1$ NMRD profiles were measured using a fast field-cycling Stelar SmartTracer relaxometer (Mede, Pv, Italy) over a continuum of magnetic field strengths from 0.00024 to 0.25 T (corresponding to 0.01–10 MHz proton Larmor frequencies). The relaxometer was operated under computer control with an absolute uncertainty in $1/T_1$ of ±1%. The temperature control was carried out using a Stelar VTC-91 airflow heater equipped with a calibrated copper–constantan thermocouple (uncertainty of ±0.1 K). Additional data points in the range 20–70 MHz were obtained using a Stelar relaxometer equipped with a Bruker WP80 NMR electromagnet adapted to variable-field measurements (15–80 MHz proton Larmor frequency). Relaxometric HSA titrations were performed using the Stelar relaxometer at 0.47 T (20 MHz) and 25 °C in dilute aqueous solutions at neutral pH. ^{17}O NMR spectra were recorded on a Bruker Avance III spectrometer (11.7 T) equipped with a 5 mm probe and a standard temperature control unit. Aqueous solutions of the complexes ($ca.$ 6–10 mM) containing 2.0% of the ^{17}O isotope (Cambridge Isotope) were used. The observed transverse relaxation rates were calculated from the signal width at half-height.

<u>X-ray crystallography</u>

Crystallographic data were collected at 100 K using a Bruker D8 Venture diffractometer equipped with a Photon 100 CMOS detector and Mo-Kα radiation (λ = 0.71073 Å) generated by an Incoatec high brilliance microfocus source equipped with Incoatec Helios multilayer optics. The software APEX3 [42] was used for collecting frames of data, indexing the reflections, and the determination of lattice parameters, SAINT[43] for integration of the intensity of reflections, and SADABS[44] for scaling and empirical absorption correction. The structure was solved by dual-space methods using the program SHELXT.[45] All non-hydrogen atoms were refined with anisotropic thermal parameters by full-matrix least-squares calculations on F^2 using the program SHELXL-2014.[46] The Squeeze program[47] was used to correct the reflection data for the diffuse scattering due to the disordered molecules present in the unit cell, which presumably correspond to a second K^+ ion required for the electroneutrality and solvent molecules. Hydrogen atoms were inserted at calculated positions and constrained with isotropic thermal parameters. The atoms from the central carboxylate group in a $DPAAA^{3-}$ moiety (C8, C9, O3 and O4) were disordered over two positions with equal occupation factors. CCDC 1518472 contains the supplementary crystallographic data for this paper. Crystal data and structure refinement details: formula: $C_{32}H_{36}KMn_2N_6O_{18}$; MW: 941.65; crystal system: monoclinic; space group: $P2_1/m$; a = 10.4813(11) Å; b = 16.0788(17) Å; c = 14.7012(16) Å; β = 103.862(4)°; V = 2405.4(4) Å^3; $F(000)$ = 966; Z = 4; $D_{calc.}$ = 1.300 g cm^{-3}; μ= 0.680 mm^{-1}; θ range = 2.37–28.31°; R_{int} = 0.0425; 43 168 measured reflections, of which 6180 were independent and 4909 were unique with $I > 2\sigma(I)$. GOF on F^2 = 0.977; R_1 = 0.0769; wR_2 (all data) = 0.2411; the largest differences peak and hole: 1.823 and −1.453 e Å^{-3}.

<u>Computational details</u>

Full geometry optimizations of the $[Mn(DPAAA)(H_2O)]^-\cdot 2H_2O$ and $[Mn(DPAPhA)(H_2O)_2]\cdot 4H_2O$ systems were performed in aqueous solution by DFT calculations at the TZVP/TPSSh[48,49] level employing the Gaussian 09 package (Revision D.01).[50] Solvent effects were included by using the polarizable continuum model (PCM), in which the solute cavity is built as an envelope of spheres centered on atoms or atomic groups with appropriate radii. In particular, we used the integral equation formalism (IEFPCM) variant as implemented in Gaussian 09.[51] No symmetry constraints have been imposed during the optimizations. The stationary points found on the potential energy surfaces as a result of geometry optimizations were tested to represent energy minima rather than saddle points *via* frequency analysis.

Acknowledgements

References

1. (*a*) B. Drahos, I. Lukes and E. Toth, *Eur. J. Inorg. Chem.*, 2012, 1975; (*b*) M. Kueny-Stotz, A. Garofalo and D. Felder-Flesch, *Eur. J. Inorg. Chem.*, 2012, 1987.

2. D. Pan, A. H. Schmieder, S. A. Wickline and G. M. Lanza, *Tetrahedron*, 2011, **67**, 8431.

3. (*a*) P. C. Lauterbur, M. H. Mendoça-Dias and A. A. Rudin, *Front. Biol. Energy*, 1978, **1**, 752; (*b*) T. J. Brady, M. R. Goldman, I. L. Pykett, F. S. Buonanno, J. P. Kistler, J. H. Newhouse, C. T. Burt, W. S. Hinshaw and G. M. Pohost, *Radiology*, 1982, **144**, 549; (*c*) M. R. Goldman, T. J. Brady, I. L.

Pykett, C. T. Burt, F. S. Buonanno, J. P. Kistler, J. H. Newhouse, W. S. Hinshaw and G. M. Pohost, *Circulation*, 1982, **66**, 1012.

4. P. Caravan, J. J. Ellison, T. J. McMurry and R. B. Lauffer, *Chem. Rev.*, 1999, **99**, 2293.

5. S. M. Rocklage, W. P. Cacheris, S. C. Quay, F. E. Hahn and K. N. Raymond, *Inorg. Chem.*, 1989, **28**, 477.

6. J. Crossgrove and W. Zheng, *NMR Biomed.*, 2004, **17**, 544.

7. (*a*) S. Cheng, L. Abramova, G. Saab, G. Turabelidze, P. Patel, M. Arduino, T. Hess, A. Kallen and M. Jhung, *J. Am. Med. Assoc.*, 2007, **297**, 1542; (*b*) T. H. Darrah, J. J. Prutsman-Pfeiffer, R. J. Poreda, M. E. Campbell, P. V. Hauschka and R. E. Hannigan, *Metallomics*, 2009, **1**, 479.

8. (*a*) E. M. Gale, I. P. Atanasova, F. Blasi, I. Ay and P. Caravan, *J. Am. Chem. Soc.*, 2015, **137**, 15548; (*b*) J. Zhu, E. M. Gale, I. Atanasova, T. A. Rietz and P. Caravan, *Chem. – Eur. J.*, 2014, **20**, 14507; (*c*) B. Phukan, A. B. Patel and C. Mukherjee, *Dalton Trans.*, 2015, **44**, 12990; (*d*) H. Su, C. Wu, J. Zhu, T. Miao, D. Wang, C. Xia, X. Zhao, Q. Gong, B. Song and H. Ai, *Dalton Trans.*, 2012, **41**, 14480.

9. (*a*) E. Molnar, N. Camus, V. Patinec, G. A. Rolla, M. Botta, G. Tircso, F. K. Kalman, T. Fodor, R. Tripier and C. Platas-Iglesias,*Inorg. Chem.*, 2014, **53**, 5136; (*b*) V. Patinec, G. A. Rolla, M. Botta, R. Tripier, D. Esteban-Gomez and C. Platas-Iglesias, *Inorg. Chem.*, 2013, **52**, 11173–11184.

10. (*a*) B. Drahos, V. Kubicek, C. S. Bonnet, P. Hermann, I. Lukes and E. Toth, *Dalton Trans.*, 2011, **40**, 1945; (*b*) B. Drahos, J. Kotek, I. Cisarova, P. Hermann, L. Helm, I. Lukes and E. Toth, *Inorg. Chem.*, 2011, **50**, 12785; (*c*) A. Forgacs, L. Tei, Z. Baranyai, I. Toth, L. Zekany and M. Botta, *Eur. J. Inorg. Chem.*, 2016, 1165.

11. B. Gallez, C. Baudelet and M. Geurts, *Magn. Reson. Imaging*, 1998, **16**, 1211.

12. (*a*) A. Takacs, R. Napolitano, M. Purgel, A. Benyei, L. Zekany, E. Brucher, I. Toth, Z. Baranyai and S. Aime, *Inorg. Chem.*, 2014,**53**, 2858; (*b*) R. Artali, Z. Baranyai, M. Botta, G. B. Giovenzana, A. Maspero, R. Negri, G. Palmisano, M. Sisti and S. Tollari, *New J. Chem.*, 2015, **39**, 539.

13. G. L. Loving, S. Mukherjee and P. Caravan, *J. Am. Chem. Soc.*, 2013, **135**, 4620.

14. S. Aime, M. Botta, E. Gianolio and E. Terreno, *Angew. Chem., Int. Ed.*, 2000, **39**, 747.

15. M. Regueiro-Figueroa, G. A. Rolla, D. Esteban-Gomez, A. de Blas, T. Rodriguez-Blas, M. Botta and C. Platas-Iglesias, *Chem. – Eur. J.*, 2014, **20**, 17300.

16. A. Forgacs, M. Regueiro-Figueroa, J. L. Barriada, D. Esteban-Gomez, A. de Blas, T. Rodriguez-Blas, M. Botta and C. Platas-Iglesias, *Inorg. Chem.*, 2015, **54**, 9576.

17. A. Nonat, P. H. Fries, J. Pecaut and M. Mazzanti, *Chem. – Eur. J.*, 2007, **13**, 8489.

18. J. Sanchiz, S. Dominguez, A. Mederos, F. Brito and J. M. Arrieta, *Inorg. Chem.*, 1997, **36**, 4108.

19. A. E. Martell, R. J. Motekaitis and R. M. Smith, *NIST Critically selected stability constants of metal complexes database, Version 8.0 for Windows, Gaithersburg*, National Institute of Standards and Technology, Standard Reference Data Program, MD, 2004.

20. B. Drahos, J. Kotek, P. Hermann, I. Lukes and E. Toth, *Inorg. Chem.*, 2010, **49**, 3224.

21. J. S. Troughton, M. T. Greenfield, J. M. Greenwood, S. Dumas, A. J. Wiethoff, J. Wang, M. Spiller, T. J. McMurry and P. Caravan, *Inorg. Chem.*, 2004, **43**, 6313.

22. A. Bianchi, L. Calabi, C. Giorgi, P. Losi, P. Mariani, D. Palano, P. Paoli, P. Rossi and B. Valtancoli, *J. Chem. Soc., Dalton Trans.*, 2001, 917.

23. J. Gao, K. Ye, M. He, W.-W. Xiong, W. Cao, Z. Y. Lee, Y. Wang, T. Wu, F. Huo, X. Liu and Q. Zhang, *J. Solid State Chem.*, 2013,**206**, 27.

24. B. Drahos, M. Pniok, J. Havlickova, J. Kotek, I. Cisarova, P. Hermann, I. Lukes and E. Toth, *Dalton Trans.*, 2011, **40**, 10131.

25. E. Balogh, Z. He, W. Hsieh, S. Liu and E. Toth, *Inorg. Chem.*, 2007, **46**, 238.

26. D. Esteban-Gómez, C. Cassino, M. Botta and C. Platas-Iglesias, *RSC Adv.*, 2014, **4**, 7094.

27. E. M. Gale, J. Zhu and P. Caravan, *J. Am. Chem. Soc.*, 2013, **135**, 18600.

28. R. Mills, *J. Phys. Chem.*, 1973, **77**, 685.

29. G. A. Rolla, C. Platas-Iglesias, M. Botta, L. Tei and L. Helm, *Inorg. Chem.*, 2013, **52**, 3268.

30. M. Regueiro-Figueroa and C. Platas-Iglesias, *J. Phys. Chem. A*, 2015, **119**, 6436.

31. L. Tei, G. Gugliotta, M. Fekete, F. K. Kalman and M. Botta, *Dalton Trans.*, 2011, **40**, 2025.

32. A. de Sa, C. S. Bonnet, C. F. G. C. Geraldes, E. Toth, P. M. T. Ferreira and J. P. Andre, *Dalton Trans.*, 2013, **42**, 4522.

33. O. M. Evbuomwan, G. Kiefer and A. D. Sherry, *Eur. J. Inorg. Chem.*, 2012, 2126.

34. E. M. Surender, S. Comby, S. Martyn, B. Cavanagh, T. C. Lee, D. F. Brougham and T. Gunnlaugsson, *Chem. Commun.*, 2016,**52**, 10858.

35. (*a*) G. Lipari and S. Szabo, *J. Am. Chem. Soc.*, 1982, **104**, 4546; (*b*) G. Lipari and S. Szabo, *J. Am. Chem. Soc.*, 1982, **104**, 4559.

36. F. Kielar, L. Tei, E. Terreno and M. Botta, *J. Am. Chem. Soc.*, 2010, **132**, 7836.

37. S. Aime, P. L. Anelli, M. Botta, M. Brocchetta, S. Canton, F. Fedeli, E. Gianolio and E. Terreno, *J. Biol. Inorg. Chem.*, 2002, **7**, 58.

38. M. Botta, S. Avedano, G. B. Giovenzana, A. Lombardi, D. Longo, C. Cassino, L. Tei and S. Aime, *Eur. J. Inorg. Chem.*, 2011, 802.

39. H. M. Irving, M. G. Miles and L. Pettit, *Anal. Chim. Acta*, 1967, **38**, 475.

40. L. Zékány and I. Nagypál, in *Computational Method for Determination of Formation Constants*, ed. D. J. Legett, Plenum, New York, 1985, p. 291.

41. D. M. Corsi, C. Platas-Iglesias, H. van Bekkum and J. A. Peters, *Magn. Reson. Chem.*, 2001, **39**, 723.

42. *APEX3 Version 2016.1*, Bruker AXS Inc., 2016.

43. *SAINT Version 8.37A*, Bruker AXS Inc., 2015.

44. G. M. Sheldrick, *SADABS Version 2014/5*, Bruker AXS Inc.

45. *SHELXT Version 2014/5*; G. M. Sheldrick, *Acta Crystallogr., Sect. A: Fundam. Crystallogr.*, 2015, **71**, 3.

46. *SHELXL Version 2014/7*; G. M. Sheldrick, Acta Crystallogr., Sect. A: Fundam. Crystallogr., 2008, 64, 112.

47. A. L. Spek, *Acta Crystallogr., Sect. C: Cryst. Struct. Commun.*, 2015, **71**, 9.

48. J. M. Tao, J. P. Perdew, V. N. Staroverov and G. E. Scuseria, *Phys. Rev. Lett.*, 2003, **91**, 146401.

49. A. Schaefer, C. Huber and R. Ahlrichs, *J. Chem. Phys.*, 1994, **100**, 5829.

50. M. J. Frisch, *et al.*, Gaussian, Inc., Wallingford CT, 2009.

51. J. Tomasi, B. Mennucci and R. Cammi, *Chem. Rev.*, 2005, **105**, 2999.